

Clustering Methods for Identifying and Modelling Areas with Similar Temperature Variations

Edoardo Otranto

Department of Social Sciences and Economics

Sapienza University of Rome

Piazzale Aldo Moro, 5; 00185 Rome

e-mail: edoardo.otranto@uniroma1.it

January 30, 2026

Abstract

This paper proposes a novel data-driven approach for identifying and modelling areas with similar temperature variations through clustering and Space-Time AutoRegressive (STAR) models. Using annual temperature data from 168 countries (1901-2022), we apply three clustering methods based on (i) warming rates, (ii) annual temperature variations, and (iii) persistence of variation signs, using Euclidean and Hamming distances. These clusters are then employed to construct alternative spatial weight matrices for STAR models. Empirical results show that distance-based STAR models outperform classical contiguity-based ones, both in-sample and out-of-sample, with the Hamming distance-based STAR model achieving the best predictive accuracy. The study demonstrates that using statistical similarity rather than geographical proximity improves the modelling of global temperature dynamics, suggesting broader applicability to other environmental and socioeconomic datasets.

Acknowledgements The author acknowledges financial support from the Italian PRIN 2022 grant "Methodological and computational issues in large-scale time series models for economics and finance" (20223725WE), funded by the European Union - Next Generation EU, Mission 4 Component 1 CUP 2J53D23003960006.

1 Introduction

Temperature change varies across countries for several reasons, including greenhouse gas emissions and geographic location. Consequently, European countries exhibit a more pronounced warming trend than those in other continents, while North America and northern regions in general have experienced strong temperature increases in recent years due to the Arctic amplification effect (Previdi et al., 2021).

Several studies have also shown that Asia and Africa have undergone substantial temperature increases, although not as pronounced as in Europe or North America, whereas Oceania exhibits the lowest warming. For example, the Food and Agriculture Organization of the United Nations report (FAO, 2025), which covers 198 countries and 39 territories, provides observed changes in land surface temperatures relative to the 1951-1980 baseline, showing that several countries have experienced increases of up to 2°C. Similarly, Shen et al. (2022) analyzed temperature trends in 146 major countries from 1980 to 2019, providing clear evidence of global surface warming with marked spatial heterogeneity and polar amplification. They found that more than 80% of global land areas have undergone significant warming, occurring more rapidly in the Northern Hemisphere than in the Southern Hemisphere. The most intense warming has been recorded in high northern latitudes, confirming Arctic amplification, while warming rates decrease toward the equator, becoming minimal or even negative. Regions with the strongest warming include Greenland (0.654°C per decade), Russia, Ukraine, Eastern Europe, Northern Canada, Northern Africa, and the Middle East, whereas areas with the weakest warming (less than 0.15°C per decade) include New Zealand, equatorial South America, Southeast Asia, and Southern Africa.

Matthews et al. (2014) examined national contributions to global temperature change through emissions, land use, and other drivers, while Ward and Mahowald (2014) demonstrated how future warming is linked to both past and ongoing emissions. At more localized scales, Caol et al. (2017) analyzed long-term observational records (1901-2015) for China, identifying persistent warming patterns; Ruosteenoja and Räisänen (2021) applied 28 global climate models to study monthly and annual mean temperatures in Finland from 1901 to 2018, successfully reproducing the observed warming; and Gil-Alana and Sauci (2019) used station data from 12 European countries to detect statistically significant warming trends, national variations, and microclimate effects.

Studying temperature trends, identifying clusters of areas with similar thermal dynamics, and developing models that account for these spatial and temporal characteristics are crucial for assessing the impacts of climate change in multiple domains, including macroeconomic (Bilal and Käenzig, 2025), financial (Naifar, 2024), and migration dynamics (McLeman and Smit, 2006).

The natural framework for analyzing temperature change is space-time modelling.¹ Since the seminal work by Cliff and Ord (1975), space-time models have been successfully extended to the ARIMA class (Pfeifer and Deutsch, 1980). Among these, the simple Space-Time AutoRegressive (STAR) model is of particular importance due to its linear structure, straightforward estimation procedure, and several desirable properties, such as its long-run steady-state equilibrium implications (LeSage and Pace, 2009).

A critical component of the STAR model is the specification of the spatial weight matrix, which determines how spatial interactions among units are represented. Typically, such weights are constructed using either contiguity or

¹For a review of these models in environmental contexts, see Le and Zidek (2006).

Zone	# Countries	% Sample	% Zone
Europe	37	4.79	93.78
Asia	38	17.18	60.21
Eurasia	5	15.40	100
Africa	46	21.99	94.94
North America	3	17.66	90.52
Central America	14	0.61	95.04
South America	13	15.12	99.53
Oceania	12	7.25	99.70
Global	168	100	87.10

Table 1: Distribution of 168 countries across geographical zones: number of countries (Column *# Countries*), percentage of area covered by the countries in the sample (*% Sample*), and percentage of global area covered by the countries in the sample compared to the corresponding zone sample (*% Zone*).

distance-based criteria (Anselin, 2013). The former approach is particularly well suited to climate studies, given the tendency of neighboring territories to exhibit similar thermal behavior.

In this paper, we analyze a large annual dataset (1901-2022) covering 168 countries, with two main objectives. First, we identify groups of countries that are similar in terms of warming rate, annual temperature variation, and the sign of change using classical clustering methods applied to various distance matrices. Second, we construct spatial weight matrices derived from these distances and clusters to estimate alternative STAR models, which we then compare to a benchmark model based on contiguity-based weights. We demonstrate that the new distance-based specifications achieve superior in-sample and out-of-sample performance.

The paper is organized as follows. Section 2 briefly describes the dataset; Section 3 presents three alternative clustering approaches for the countries considered in this study, based on similarity in annual warming rates (Subsection 3.1), similarity in temperature variations (Subsection 3.2), and similarity in the sign of temperature variations (Subsection 3.3). These clusters and their associated distance measures are then used to extend the STAR model specification, whose performance is compared with that of the baseline contiguity-based STAR model in both in-sample and out-of-sample contexts (Section 4). Section 5 concludes with some final remarks. The final Appendix provides the complete list of the countries analyzed, with the corresponding cluster to which they belong according to the three alternative criteria illustrated in Section 3.

2 The Dataset

The dataset used in this study is freely available on Kaggle.² It contains annual average temperature series for 168 countries spanning the years 1901-2022, for a total of 20,496 observations.

Table 1 summarizes the distribution of countries across the main geographical regions. The dataset includes a varying number of countries per region, although the emphasis is naturally placed on the total area covered by the included states. The third column of the table reports the percentage of the sample area represented by each region. With the exception of Asia, all regions cover nearly the entire geographic area (last column), with percentages exceeding 90%. The transcontinental Eurasian region (comprising Russia, Turkey, Azerbaijan, Georgia, and Kazakhstan) is fully covered. The only underrepresented region is Asia, where missing data for China and India lead to a coverage rate of 60%. The sample accounts for 87.10% of the total global land area.

Our analysis is conducted at the country level, and therefore the absence of major states such as China and India does not directly affect the estimation. Nevertheless, it is important to consider the behavior of regions adjacent to these two countries, which rank first and third among the largest emitters of greenhouse gases—widely recognized as the primary anthropogenic driver of climate change—accounting for 32.88% and 6.99% of global emissions, respectively (the United States ranks second with 12.60%).³

3 Clusters of Countries with Similar Temperature Changes

The first step of our analysis involves clustering the 168 countries based on several criteria derived from their temperature dynamics over 122 years. The characteristics of interest are the rate of warming (hereafter, Clustering A), the temperature variations (Clustering B), and the persistence of the sign of these variations (Clustering C). These features can be quantified using three different statistical tools: the slope of an estimated linear trend, the first-difference operator, and the sequences of signs. The three approaches are presented in the following subsections, along with the corresponding clustering results.

3.1 Clustering A: Similar Annual Warming Rates

The 168 time series display a clear linear trend. Figure 1 illustrates the temperature dynamics of six countries, where the dotted line represents the esti-

²The dataset can be downloaded from <https://www.kaggle.com/datasets/palinatx/mean-temperature-for-countries-by-year-2014-2022>. It was scraped from the World Bank Climate Knowledge Portal (<https://climateknowledgeportal.worldbank.org/>) and includes data for all available countries from 1901 to 2022. Unfortunately, data for some major countries, such as China and India, are not available for this period.

³Emission data are available at <https://www.worldometers.info/co2-emissions/>.

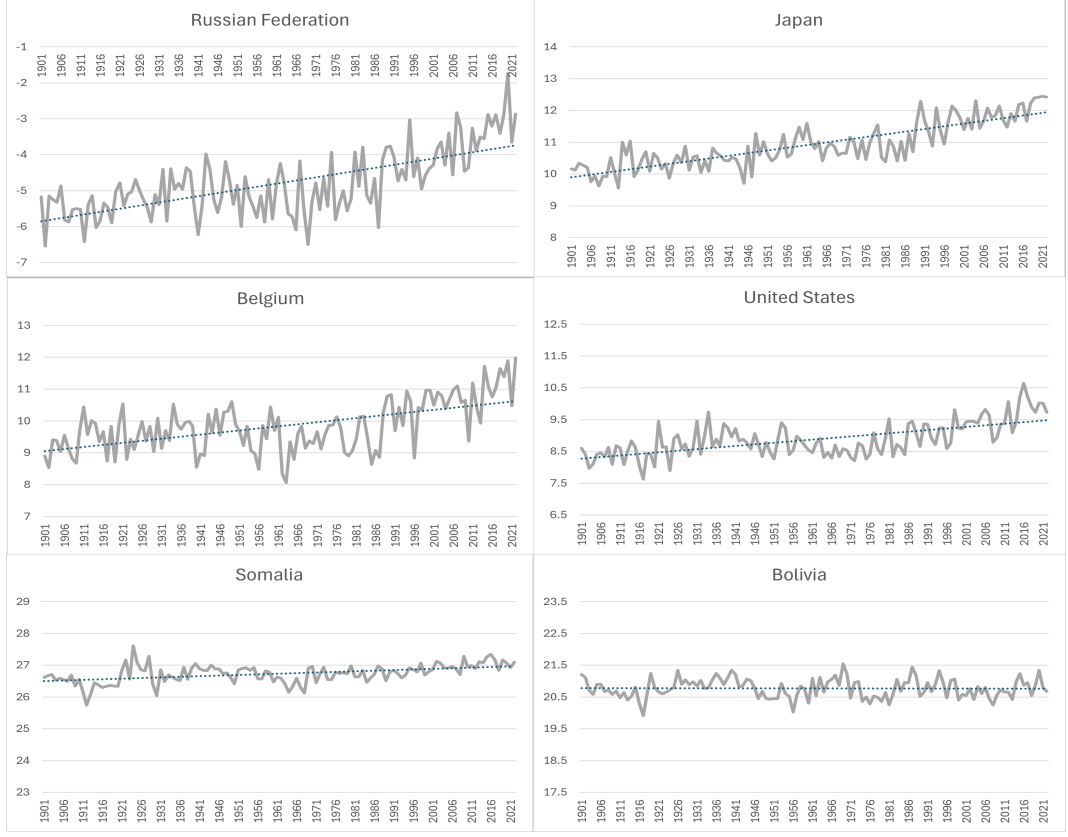


Figure 1: Temperature time series (solid gray lines) of six countries and their corresponding linear trends (dotted black lines).

mated linear trend.⁴ The increase in temperature is approximately linear, but the slopes differ substantially: the Russian Federation and Japan exhibit steep slopes, reflecting a faster rate of warming; Belgium shows a moderate slope; the United States a milder one; while Somalia and, especially, Bolivia display almost flat trends.

The first clustering procedure identifies groups of countries with similar trend slopes. For each country, we estimate a simple linear regression model, where $y_{i,t}$ denotes the temperature of the i -th country in year t ($i = 1, \dots, 168$; $t = 1, \dots, 122$):

$$y_{i,t} = a_i + b_i t + \varepsilon_{i,t} \quad (1)$$

where a_i is the intercept, b_i is the slope parameter (interpreted as the annual warming rate), and $\varepsilon_{i,t}$ are zero-mean homoskedastic and uncorrelated errors. The distance between countries i and j is computed as the classical Euclidean

⁴For comparison, the same range on the y -axis (temperature) is set to 6°C.

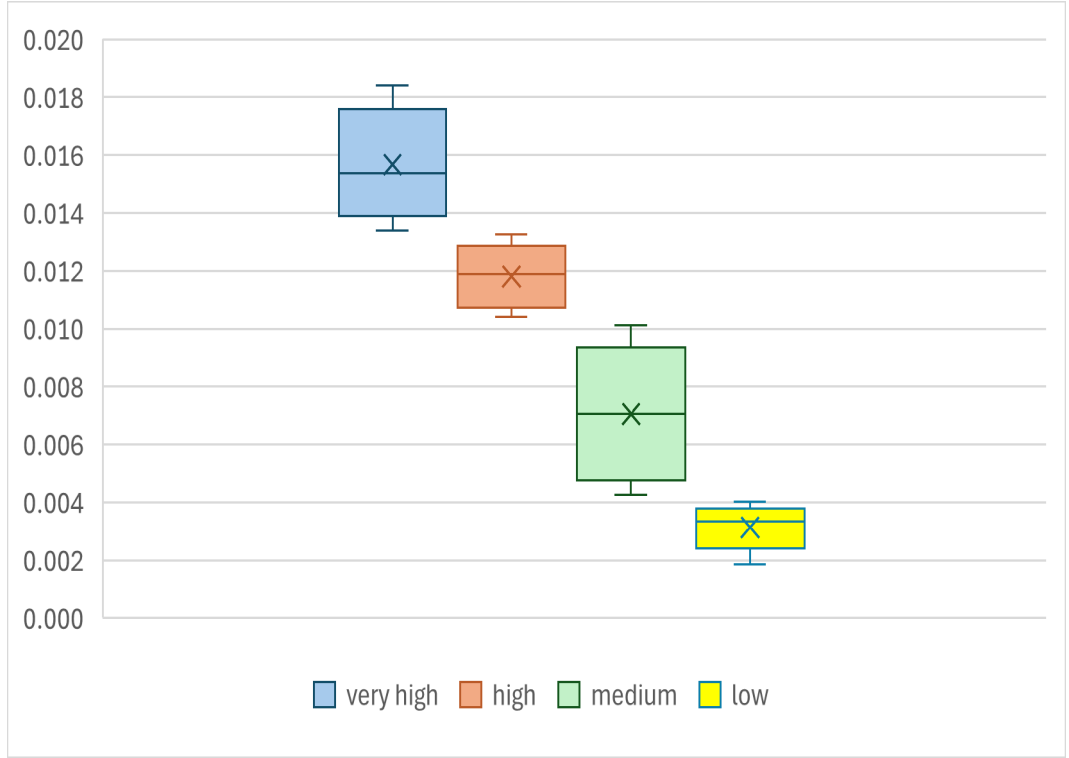


Figure 2: Boxplots of the estimated slope coefficients for each cluster. The cross indicates the mean slope within the corresponding cluster.

distance between the estimated slope coefficients, which in this case has the closed form:

$$d_{ij}^b = |b_i - b_j| \quad (2)$$

An agglomerative clustering algorithm with the average linkage criterion is then applied (see, e.g., Yang, 2017). The number of clusters is determined from the dendrogram, based on the distance at which clusters merge.

In six cases, the slope coefficient b_i is not significantly different from zero at the 5% level, suggesting no temperature increase during the observed period. These countries are Bolivia (South America; see Figure 1), Timor-Leste (Asia), Madagascar (Africa), and Kiribati, Nauru, and the Solomon Islands (Oceania). They are excluded from the clustering, which identifies four groups.

Figure 2 shows that the four clusters are well separated and can be interpreted as very high, high, medium, and low warming rates, respectively. The very high slope group includes countries with annual warming rates between 0.013 and 0.018 (mean = 0.016); the mean slopes of the remaining clusters are 0.012, 0.007, and 0.003, respectively. The highest rate is observed in Mongolia, likely influenced by its proximity to China.

	very high	high	medium	low	null	
Europe	19	14	4	0	0	37
Asia	14	6	17	0	1	38
Eurasia	2	2	1	0	0	5
Africa	6	3	29	7	1	46
North America	1	1	1	0	0	3
Central America	2	5	7	0	0	14
South America	0	1	8	3	1	13
Oceania	0	1	4	4	3	12
	44	33	71	14	6	168

Table 2: Distribution of 168 countries by geographical zone and warming-rate cluster.

Table 2 displays the distribution of countries by geographical region and warming-rate cluster (including the *null* group of six countries with statistically insignificant slopes). European and Asian countries dominate the high and very high clusters, while South America and Oceania exhibit the lowest rates. Weighting countries by land area provides a more accurate picture of territorial influence (Figure 3). Eurasia’s inclusion of the Russian Federation results in almost complete dominance of the very high cluster in that region. The figure clearly indicates that Europe, Asia, Eurasia, and North America show the strongest warming-consistent with findings on Arctic amplification and greenhouse gas effects-while Africa presents moderate variability and Central/South America and Oceania exhibit lower or even null warming. A similar observation made for Eurasia holds true for Oceania, where the predominant *medium* warming is due to Australia’s classification.

3.2 Clustering B: Similar Temperature Variations

A complementary clustering approach examines the similarity of annual temperature variations to identify countries experiencing similar fluctuations over time. The goal is to determine whether comparable patterns occur across specific geographical regions. Unlike the previous classification, this clustering does not imply a natural order (e.g., very high, high, medium), since the magnitude of temperature variation changes over time: two countries may have similar average variability but differ in yearly dynamics.

We compute first differences of the temperature series using the operator Δ :

$$\Delta y_{i,t} = y_{i,t} - y_{i,t-1}$$

Clustering is again performed using an agglomerative algorithm with average linkage and the Euclidean distance:

$$d_{i,j}^\Delta = \sqrt{\sum_{t=2}^{122} (\Delta y_{i,t} - \Delta y_{j,t})^2} \quad i, j = 1, \dots, 168 \quad (3)$$

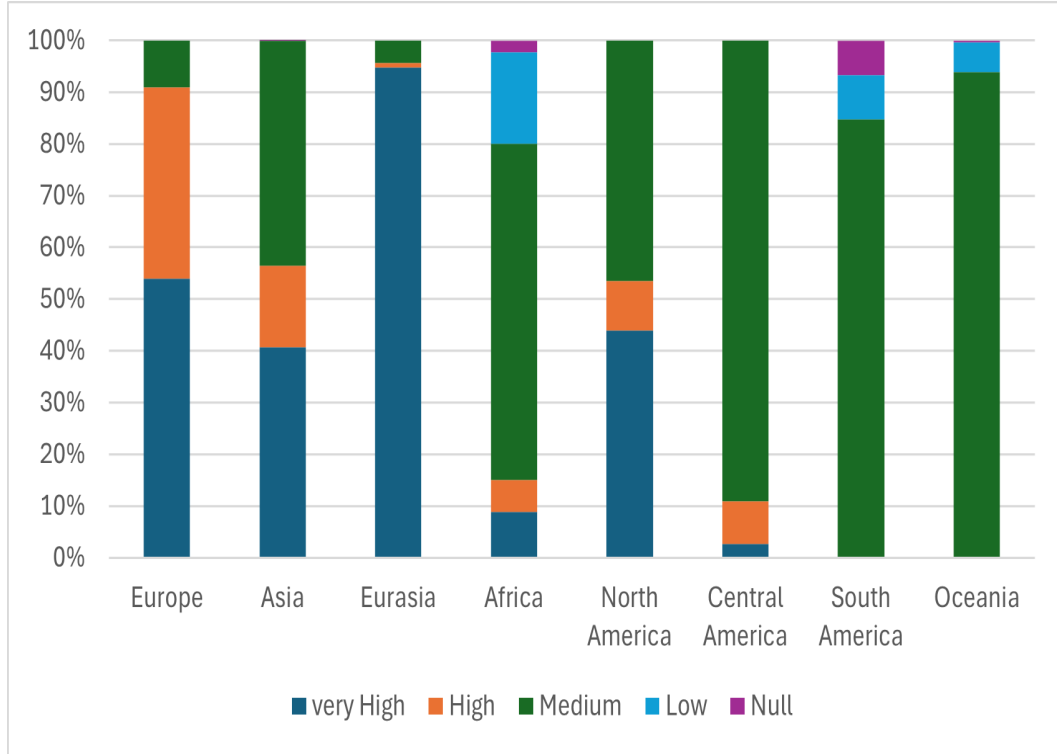


Figure 3: Distribution of warming-rate clusters across geographical zones.

Five main clusters are identified, while three Arctic-proximate countries (Canada, Iceland, and the Russian Federation) exhibit idiosyncratic behavior and are not assigned to any cluster.

The first cluster (16 countries) is centered in the Middle East, including most of the Arabian Peninsula (except Yemen and Oman) and nearby Eurasian/Asian countries, plus Egypt and Cyprus. The mean temperature change is 0.011 with a standard deviation (SD) of 0.637. A second, smaller cluster (5 countries in Central Asia) comprises Uzbekistan, Turkmenistan, Tajikistan, Kazakhstan, and Kyrgyzstan, characterized by higher average variations (mean = 0.018, SD = 0.867). Two additional clusters correspond to Europe: a southeastern group (13 countries) with the highest mean variation (0.019, SD = 0.731), and a northwestern/Baltic group (12 countries) with lower mean variation (0.017) but the largest variability (SD = 0.975). Finally, a large heterogeneous cluster of 119 countries, labeled *Miscellanea*, shows low average variation (0.007) and low variability (SD = 0.348).

Table 3 shows the cross-distribution of Clustering A and Clustering B. The geographically defined groups in Clustering B correspond mainly to the medium-to-very-high warming-rate clusters in Clustering A. Similarly, two of the three

Clustering B	Clustering A					13
	very high	high	medium	low	null	
SE Europe	5	6	2	0	0	13
NW and Baltic Europe	5	7	0	0	0	12
Middle East	7	7	2	0	0	16
Central Asia	4	1	0	0	0	5
Miscellanea	21	12	66	14	6	119
Idiosyncratic	2	0	1	0	0	3
	44	33	71	14	6	168

Table 3: Distribution of 168 countries by Clustering A (warming rate) and Clustering B (temperature variation).

idiosyncratic countries in Clustering B (Canada and Russia) also exhibit very high annual warming rates. The *Miscellanea* group spans all categories in Clustering A.

3.3 Clustering C: Persistence of the Sign of Variations

The magnitude of annual temperature variation can be difficult to compare across countries, as patterns are often heterogeneous; hence the large and geographically mixed *Miscellanea* cluster. An alternative way to capture similarity is to analyze the sign of annual differences (increase or decrease) and their persistence over time.

To measure dissimilarity, we adopt the Hamming distance, a metric introduced by Hamming (1950) in coding theory to detect and correct errors in programming codes. Denoting $s_{i,t}$ as the t -th value (1 or 0) of the string \mathbf{s}_i , representing the sign of the temperature change of country i between years $t-1$ and t , the Hamming distance between countries i and j is defined as:

$$d_{ij}^H = \sum_{t=2}^{122} |s_{i,t} - s_{j,t}| \quad (4)$$

This distance equals the number of differing positions between the binary vectors \mathbf{s}_i and \mathbf{s}_j . Clustering is then performed using the standard agglomerative algorithm.

This analysis yields 12 clusters and 20 idiosyncratic countries. Most clusters show clear geographic coherence. The largest includes almost all European countries (34 of 37), except for Malta (which forms a Central Mediterranean cluster with Tunisia), Cyprus (which belongs to the Middle East group), and Iceland (idiosyncratic). Four clusters correspond to Asia: the Middle East and Caucasus (18 countries), Southeast Asia (13), Central Asia (8), and East Asia (Japan and South Korea). In Africa, 42 of 46 countries belong to two clusters-West Africa (16) and Southern/Eastern Africa (26)-while North Africa exhibits a distinct pattern (e.g., Tunisia and Libya are exceptions). In the Americas, northern countries behave idiosyncratically, while most Central and

South American nations form a broad cluster of 22 countries; Peru and Ecuador (northwestern South America) form a small cluster, as do Chile and Argentina (southern South America). Uruguay stands alone as idiosyncratic. Finally, in Oceania, most countries show independent behavior, with only three Polynesian and Melanesian islands forming a small cluster.

Clustering C can be viewed as a disaggregation of Clustering B. As shown in Table 4, excluding the *Miscellanea* group, each Clustering B column corresponds roughly to a single Clustering C row, while the *Miscellanea* cluster is subdivided among the 12 clusters and idiosyncratic cases of Clustering C.

Clustering C		Clustering B		Clustering A		Clustering C	
		SE Europe	NW and Baltic Europe	Middle East	Central Asia	Miscellanea	idiosyncratic
Europe	13	12	0	0	9	9	0
Central Mediterranean	0	0	0	0	2	2	0
Middle East and Caucasus	0	0	16	0	2	0	18
Central Asia	0	0	0	5	3	0	8
E Asia	0	0	0	0	2	0	2
SE Asia	0	0	0	0	13	0	13
SE Africa	0	0	0	0	26	0	26
W Africa	0	0	0	0	16	0	16
Central and South America	0	0	0	0	22	0	22
NW South America	0	0	0	0	2	0	2
S South America	0	0	0	0	2	0	2
Polynesia and Melanesia	0	0	0	0	3	0	3
idiosyncratic	0	0	0	0	17	3	20
	13	12	16	5	119	3	168

Table 4: Distribution of 168 countries by Clustering B (temperature variation) and Clustering C (persistence of the sign of variation).

4 STAR Models with Distance-Based Weights

A STAR model incorporates both temporal and spatial dimensions within its autoregressive terms. It is among the most widely used frameworks for analysing time series associated with spatial units, as their geographical interdependence affects the dynamics of the individual series.

Let x denote a stationary variable observed over N spatial units and T time periods. In its simplest and most common specification, considering one lag in both dimensions, the model can be written as:

$$x_{i,t} = c_i + \phi_i x_{i,t-1} + \psi_i \sum_{j=1}^N w_{ij} x_{j,t-1} + \varepsilon_{i,t} \quad i = 1, \dots, N; t = 1, \dots, T \quad (5)$$

where c_i is a constant, ϕ_i the temporal autoregressive coefficient, and ψ_i the spatial autoregressive coefficient; $\varepsilon_{i,t}$ denotes a zero-mean uncorrelated disturbance. The known values w_{ij} are the elements of a spatial weight matrix, with zeros on the diagonal, representing for each row i the degree of influence of the other spatial units on unit i .

As mentioned, the choice of the spatial weight matrix plays a crucial role in determining the performance of the model. Frequently, contiguity-based weights are employed, assigning a weight of $1/m$ to each of the m immediate neighbours and zero otherwise. However, improved results can often be achieved by deriving the weights from a distance measure directly related to the phenomenon under investigation (see, e.g., Anselin and Rey, 2014), explicitly defining weights inversely proportional to distance. Given the distance $d_{ij} \leq N$ between units i and j , the corresponding spatial weights can be derived in two steps. First, the unnormalised weights are computed as:

$$w_{ij}^* = \begin{cases} \frac{N-d_{ij}}{N} & \text{if } i \neq j \\ 0 & \text{otherwise} \end{cases} \quad (6)$$

Then the weights are normalised as:

$$w_{ij} = \frac{w_{ij}^*}{\sum_{j=1}^N w_{ij}^*} \quad (7)$$

Given the close connection between the three clustering procedures described earlier and the geographical distribution of countries, we propose to replace d_{ij} in (6) with the distances (2), (3), and (4) to obtain the set of spatial weights. This yields six distinct weight matrices:

- Three matrices are obtained by considering only the distances between countries belonging to the same cluster, assigning zero weights otherwise.⁵ The corresponding STAR models with cluster-based weights are denoted STAR_{cA} , STAR_{cB} , and STAR_{cc} , respectively.

⁵For example, under Clustering C, Brazil receives a non-zero weight with Bolivia because they belong to the same cluster, while it receives a zero weight with Argentina despite their geographical proximity.

In-sample							
	STAR _{NN}	STAR _{cA}	STAR _{cB}	STAR _{cC}	STAR _{dA}	STAR _{dB}	STAR_{dC}
FN	4491.5	4490.6	4486.8	4489.2	4485.8	4483.2	4480.3
Out-of-sample							
	STAR _{NN}	STAR _{cB}	STAR _{cC}	STAR _{cA}	STAR _{dB}	STAR_{dC}	STAR_{dA}
FN	658.3	656.2	655.9	654.1	654.2	653.8	650.6
pv	0.000	0.000	0.001	0.001	0.001	0.012	1.000

Table 5: Frobenius norm for in-sample and out-of-sample evaluation. For the out-of-sample case, models are ordered from left to right according to the sequence of eliminations in the MCS procedure, down to the best-performing model. The last row reports the associated p-values (pv). Best-performing models are in bold.

- Three matrices are obtained by considering all distances (2), (3), and (4) and applying equations (6)-(7). The corresponding STAR models with distance-based weights are denoted STAR_{dA}, STAR_{dB}, and STAR_{dC}, respectively.

Each of the six proposed models is estimated equation by equation using OLS, since the number of spatial units exceeds the number of time periods and a joint estimation would be affected by collinearity issues (D'Urso et al., 2022).⁶ The time series are made stationary by first differencing ($x_{i,t} = \Delta y_{i,t}$ in equation (5)). We then evaluate the performance of the models both in-sample and out-of-sample, comparing them with a baseline STAR model whose weights are derived from a contiguity matrix (non-zero weights only for *nearest neighbours*; Anselin, 2013). This baseline model is denoted STAR_{NN}.⁷

The in-sample evaluation compares fitted and observed temperatures using the Frobenius norm, which is equivalent to the Mean Squared Error in the univariate case. Denoting fitted temperatures by $\hat{y}_{i,t}$, and letting $\mathbf{Y} = \{y_{i,t}\}$ and $\hat{\mathbf{Y}} = \{\hat{y}_{i,t}\}$ denote the $N \times T$ matrices of observed and fitted temperatures, respectively, the Frobenius norm is defined as:

$$FN = \text{trace} \left[(\mathbf{Y} - \hat{\mathbf{Y}})'(\mathbf{Y} - \hat{\mathbf{Y}}) \right] \quad (8)$$

The upper panel of Table 5 reports the FN values for the in-sample evaluation. All models using distance-based matrices outperform the baseline model. Among the cluster-based models (subscript *c*), clustering B performs best; among those with distance-based weights (subscript *d*), STAR_{dC} achieves the lowest loss, outperforming all other models.

Statistical climate models are most relevant when assessed in terms of their predictive ability. To this end, we designed the following out-of-sample experiment:

⁶In practice, we assume uncorrelated disturbances across spatial units, such that their relationships are fully captured by the spatial autoregressive component of (5).

⁷Estimation results are available upon request.

1. consider the 168 time series from 1901 to 2000;
2. estimate the seven models on this reduced dataset;
3. use the estimated models to forecast the next 22 values;
4. compare observed data for 2001-2022 with forecasts using the FN in (8).

The lower panel of Table 5 reports the FN values for the out-of-sample evaluation. Again, all distance-based STAR models outperform the baseline. In this case, $STAR_{dA}$ yields the best performance, with an FN value 7.7 points lower than $STAR_{NN}$ and 3.2 points lower than the second-best model ($STAR_{dC}$).

To formally test whether differences in predictive accuracy are statistically significant, we apply the Model Confidence Set (MCS) procedure (Hansen et al., 2011). This iterative testing approach identifies, for a given significance level and loss function, the subset of models with equal predictive ability.⁸ At the 1% significance level, Table 5 shows that $STAR_{dC}$ belongs to the best-performing set together with $STAR_{dA}$.

In summary, the proposed distance-based STAR models outperform the classical contiguity-based STAR specification both in-sample and out-of-sample. Among them, $STAR_{dC}$ -based on the Hamming distance between the signs of temperature variations-achieves the lowest FN loss in-sample and ranks among the best models out-of-sample.

5 Final Remarks

Statistical models for capturing and forecasting climate change represent a rapidly growing area of research. In this study, we focus on one of the most widely used space-time models, the STAR model, which is both flexible and straightforward to estimate. A key element in this framework is the spatial weight matrix, which encodes the relationships and mutual influence among countries. In the context of temperature variations, a natural choice is to rely on proximity among neighboring countries.

Our proposal adopts a data-driven approach, selecting the most similar countries through clustering methods that account for three main characteristics: similarity in annual warming rates, similarity in temperature variations, and similarity in the sign of temperature changes. For the first two characteristics, we employ the classical Euclidean distance to perform clustering, while for the latter, we use the Hamming distance, originally developed in computer science for error detection in coding. After verifying that all three clustering procedures yield clusters that correspond to specific geographic areas, we modify the weight matrix of the classical STAR model by considering either only intra-cluster relationships or the full distance matrices. Among these alternatives, the weight

⁸We refer to Hansen et al. (2011) for technical details. The test statistic used here is the semi-quadratic statistic, but the alternative range statistic proposed by the same authors yields identical results. Following their recommendation, the variance of the statistic is obtained using 10,000 bootstrap replications.

matrix based on the Hamming distance provides the best performance in both in-sample and out-of-sample evaluations.

Clustering has previously been applied in STAR models for various purposes. For instance, Otranto and Mucciardi (2019) use clustering procedures to reduce the number of unknown coefficients in STAR models, thereby achieving flexible yet parsimonious parameterizations. Similarly, D'Urso et al. (2022) apply fuzzy clustering to the parameters of each STAR equation to identify groups of countries with similar dynamics in workplace mobility trends-a procedure conceptually inverse to ours, where clustering is used to define the spatial weight matrix itself.

The primary aim of this work was to propose a novel approach to enhance the fitting and forecasting performance of one of the most widely used models in climate analysis. However, this methodology could be extended to alternative space-time models for climate change (see, e.g., Kyriakidis and Journel, 1999; Le and Zidek, 2006). It may be particularly interesting to apply this approach to other climate-related datasets, not limited to temperature, but including variables such as greenhouse gas emissions, industrialization levels, precipitation, or river flows. Moreover, exploring alternative clustering procedures, such as fuzzy clustering as in D'Urso et al. (2022), represents a promising avenue for further research.

Funding Sources

The author gratefully acknowledges the *Italian PRIN 2022* grant (20223725WE) “Methodological and computational issues in large-scale series models for economics and finance”.

A Countries and Clusters

In this Appendix, we provide an alphabetical list of the countries included in the dataset, along with their corresponding geographical region (see Table 1) and the cluster assignments according to Clustering A, B, and C.

Legenda of the clusters:

Clustering A:

1=medium, 2=high, 3=very high, 4=low, 5=null.

Clustering B:

1=Middle East, 2=Central Asia, 3=Southeastern (SE) Europe, 4=Northwestern (NW) and Baltic Europe, 5=Miscellanea, 6=idiosyncratic.

Clustering C:

1=Central Mediterranean, 2=northwestern part (NW) of South America, 3=Central Asia, 4=Polynesia and Melanesia, 5=East (E) Asia, 6=southern (S) South America, 7=Europe, 8=Central and South America, 9=Southern and Eastern

(SE) Africa, 10=West (W) Africa, 11=Southeast (SE) Asia, 12=Middle East and Caucasus, 13=idiosyncratic.

Country	Geographical zone	Clustering A	Clustering B	Clustering C
Afghanistan	Asia	2	5	3
Albania	Europe	1	3	7
Algeria	Asia	1	5	13
Andorra	Europe	3	5	7
Angola	Africa	1	5	13
Argentina	South America	1	5	6
Armenia	Asia	2	1	12
Australia	Oceania	1	5	13
Austria	Europe	3	3	7
Azerbaijan	Eurasia	2	1	12
Bahamas,	Central America	2	5	8
Bahrain	Asia	3	1	12
Bangladesh	Asia	1	5	11
Barbados	Central America	2	5	8
Belarus	Europe	3	4	7
Belgium	Europe	2	4	7
Belize	Central America	1	5	8
Benin	Africa	1	5	10
Bhutan	Asia	1	5	11
Bolivia	South America	5	5	8
Botswana	Africa	1	5	9
Brazil	South America	1	5	8
Bulgaria	Europe	2	3	7
Burundi	Africa	1	5	9
Cambodia	Asia	1	5	11
Cameroon	Africa	4	5	10
Canada	North America	3	6	13
Central African Republic	Africa	1	5	9
Chad	Africa	1	5	9
Chile	South America	4	5	6
Colombia	South America	1	5	8
Comoros	Africa	4	5	9
Congo, Dem. Rep.	Africa	4	5	9

Country	Geographical zone	Clustering A	Clustering B	Clustering C
Costa Rica	Central America	1	5	8
Cote d'Ivoire	Africa	1	5	10
Croatia	Europe	3	3	7
Cuba	Central America	2	5	8
Cyprus	Europe	2	1	12
Denmark	Europe	2	4	7
Djibouti	Africa	1	5	9
Dominica	Central America	3	5	8
Dominican Republic	Central America	3	5	8
Ecuador	South America	4	5	2
Egypt	Africa	1	1	12
Eritrea	Africa	1	5	9
Estonia	Europe	3	4	7
Eswatini	Africa	3	5	9
Ethiopia	Africa	1	5	9
Fiji	Oceania	4	5	4
Finland	Europe	2	4	7
France	Europe	3	5	7
Gabon	Africa	1	5	10
Gambia	Africa	1	5	10
Georgia	Eurasia	2	1	12
Germany	Europe	3	4	7
Ghana	Africa	1	5	10
Greece	Europe	1	3	7
Grenada	Central America	2	5	8
Guatemala	Central America	1	5	8
Guinea	Africa	1	5	10
Guinea Bissau	Africa	1	5	10
Guyana	South America	1	5	8
Haiti	Central America	2	5	8
Honduras	Central America	1	5	8
Hungary	Europe	3	3	7
Iceland	Europe	1	6	13

Country	Geographical zone	Clustering A	Clustering B	Clustering C
Indonesia	Asia	1	5	11
Iran, Islamic Rep.	Asia	3	5	3
Iraq	Asia	3	1	12
Israel	Asia	2	1	12
Italy	Europe	3	5	7
Jamaica	Central America	1	5	8
Japan	Asia	3	5	5
Jordan	Asia	3	1	12
Kazakhstan	Asia	3	2	3
Kenya	Africa	3	5	9
Kiribati	Oceania	5	5	13
Korea-South	Asia	3	5	5
Kuwait	Asia	3	1	12
Kyrgyz Republic	Asia	3	2	3
Latvia	Europe	3	4	7
Lebanon	Asia	3	1	12
Lesotho	Africa	3	5	9
Liberia	Africa	4	5	10
Libya	Africa	1	5	13
Liechtenstein	Europe	3	5	7
Luxembourg	Europe	3	4	7
Madagascar	Africa	5	5	9
Malawi	Africa	1	5	9
Malaysia	Asia	1	5	11
Maldives	Asia	1	5	11
Mali	Africa	1	5	10
Malta	Europe	3	5	1
Mauritania	Africa	1	5	10
Mauritius	Africa	1	5	9
Mexico	North America	2	5	13
Moldova	Europe	2	3	7
Monaco	Europe	3	5	7
Mongolia	Asia	3	5	13
Montenegro	Europe	2	3	7

Country	Geographical zone	Clustering A	Clustering B	Clustering C
Mozambique	Africa	1	5	9
Myanmar	Asia	1	5	11
Nauru	Oceania	5	5	13
Nepal	Asia	1	5	11
Netherlands	Europe	2	4	7
New Zealand	Oceania	1	5	13
Nicaragua	Central America	1	5	8
Niger	Africa	1	5	10
Nigeria	Africa	4	5	10
Norway	Europe	2	4	7
Oman	Asia	1	5	12
Pakistan	Asia	1	5	3
Palau	Oceania	1	5	13
Panama	Central America	1	5	8
Papua New Guinea	Oceania	4	5	13
Paraguay	South America	4	5	8
Peru	South America	1	5	2
Philippines	Asia	1	5	11
Poland	Europe	2	4	7
Portugal	Europe	3	5	7
Qatar	Asia	3	1	12
Romania	Europe	2	3	7
Russian Federation	Eurasia	3	6	13
Rwanda	Africa	2	5	9
Samoa	Oceania	2	5	4
Saudi Arabia	Asia	2	1	12
Senegal	Africa	1	5	10
Serbia	Europe	2	3	7
Seychelles	Africa	1	5	9
Sierra Leone	Africa	4	5	10
Singapore	Asia	1	5	11
Slovak Republic	Europe	2	3	7
Slovenia	Europe	3	3	7
Solomon Islands	Oceania	5	5	13

Country	Geographical zone	Clustering A	Clustering B	Clustering C
Somalia	Africa	4	5	9
South Africa	Africa	3	5	9
South Sudan	Africa	2	5	9
Spain	Europe	3	5	7
Sri Lanka	Asia	1	5	11
Sudan	Africa	1	5	9
Suriname	South America	1	5	8
Sweden	Europe	2	4	7
Switzerland	Europe	3	5	7
Syrian Arab Republic	Asia	2	1	12
Tajikistan	Asia	2	2	3
Tanzania	Africa	2	5	9
Thailand	Asia	1	5	11
Timor Leste	Asia	5	5	13
Togo	Africa	1	5	10
Tonga	Oceania	1	5	4
Trinidad And Tobago	South America	2	5	8
Tunisia	Africa	3	5	1
Turkey	Eurasia	1	1	12
Turkmenistan	Asia	3	2	3
Tuvalu	Oceania	4	5	13
Uganda	Africa	3	5	9
Ukraine	Europe	3	3	7
United Arab Emirates	Asia	3	1	12
United Kingdom	Europe	1	5	7
United States	North America	1	5	13
Uruguay	South America	1	5	13
Uzbekistan	Asia	3	2	3
Vanuatu	Oceania	4	5	13
Venezuela, Rb	South America	1	5	8
Vietnam	Asia	1	5	11
Yemen, Rep.	Asia	1	5	12
Zambia	Africa	1	5	9
Zimbabwe	Africa	1	5	9

References

Anselin, L., 2013. Spatial Econometrics: Methods and Models, vol. 4. Springer Science & Business Media.

Anselin, L., Rey, S., 2014. Modern Spatial Econometrics in Practice, A Guide to GeoDa, GeoDaSpace and PySAL. GeoDa Press, Chicago, IL.

Bilal, A., Känzig, D., 2025. The macroeconomic impact of climate change: Global vs. local temperature. NBER Working Paper 32450.

Caol, L., Yan, Z., Zhao, P., Zhu, Y., Yu, Y., Tang, G., Jones, P., 2017. Climatic warming in China during 1901-2015 based on an extended dataset of instrumental temperature records. *Environmental Research Letters* 12, 064005.

Cliff, A., Ord, J., 1975. Space-time modelling with an application to regional forecasting. *Transactions of the Institute of British Geographers* 64, 119–128.

D'Urso, P., Mucciardi, M., Otranto, E., Vitale, V., 2022. Community mobility in the European regions during COVID-19 pandemic: A partitioning around medoids with noise cluster based on space-time autoregressive models. *Spatial Statistics* 49, 100531.

FAO, 2025. Temperature change statistics 1961-2024: Global, regional and country trends. FAOSTAT Analytical Brief 101. Food and Agricultural Organization of the United Nations.

Gil-Alana, L., Sauci, L., 2019. Temperatures across Europe: evidence of time trends. *Climatic Change* 157, 355–364.

Hamming, R., 1950. Error detecting and error correcting codes. *The Bell System Technical Journal* 29, 147–160.

Hansen, P.R., Lunde, A., Nason, J.M., 2011. The model confidence set. *Econometrica* 79, 453–497.

Kyriakidis, P., Journel, A., 1999. Geostatistical space-time models: A review. *Mathematical Geology* 31, 651–683.

Le, N., Zidek, J., 2006. Statistical Analysis of Environmental Space-Time Processes. Springer.

LeSage, J., Pace, R., 2009. Introduction to Spatial Econometrics. Chapman & Hall, Boca Raton.

Matthews, H., Gtaham, T., Keverian, S., Lamontagne, C., Seto, D., Smith, T., 2014. National contributions to observed global warming. *Environmental Research Letters* 9, 014010.

McLeman, R., Smit, B., 2006. Migration as an adaptation to climate change. *Climate Change* 76, 31–53.

Naifar, N., 2024. Climate Change and Finance. Springer.

Otranto, E., Mucciardi, M., 2019. Clustering space-time series: FSTAR as a flexible star approach. *Advances in Data Analysis and Classification* 13, 175–199.

Pfeifer, P., Deutsch, S., 1980. A three-stage iterative procedure for space-time modeling. *Technometrics* 22, 35–47.

Previdi, M., Smith, K.L., Polvani, L.M., 2021. Arctic amplification of climate change: a review of underlying mechanisms. *Environmental Research Letters* 16, 093003.

Ruosteenoja, K., Räisänen, J., 2021. Evolution of observed and modelled temperatures in Finland in 1901-2018 and potential dynamical reasons for the differences. *International Journal of Climatology* 41, 3374–3390.

Shen, B., Song, S., Zhang, L., Whang, Z., Ren, C., Li, Y., 2022. Temperature trends in some major countries from the 1980s to 2019. *Journal of Geographical Sciences* 32, 79–100.

Ward, D., Mahowald, N., 2014. Contributions of developed and developing countries to global climate forcing and surface temperature change. *Environmental Research Letters* 9, 074008.

Yang, Y., 2017. Chapter 3 - Temporal data clustering, in: Yang, Y. (Ed.), *Temporal Data Mining Via Unsupervised Ensemble Learning*. Elsevier, pp. 19–34.